Journal of Applied Mechanics Vol.7,pp.527-534 (August 2004) JSCE

Axisymmetric Bifurcations of Metals with Tangential-Subloading Surface Model

Mehdi KHOJASTEHPOUR*, Koichi HASHIGUCHI** and Yukitaka MURAKAMI***

* JSPS Postdoctoral Fellow, Dept. Mechanical Eng. Sci., Kyushu University
Hakozaki, Higashi-ku, Fukuoka 812-8581
** Dr. Eng. and Dr. Agr., Professor, Dept. Bioproduction Environmental. Sci., Kyushu University
Hakozaki, Higashi-ku, Fukuoka 812-8581
*** Dr. Eng., Professor, Dept. Mechanical Eng. Sci, Kyushu University
Hakozaki, Higashi-ku, Fukuoka 812-8581

This article discusses about localized bifurcation corresponding to shear band formation and diffuse bifurcation modes of deformation, such as necking and bulging, for a cylindrical metallic specimen subjected to tensile or compressive loading under axisymmetric deformations. Further, conditions for the shear band formation, the diffuse bifurcations, and the long and short wavelength bifurcation are discussed in relation to material properties and their state of stress. We employ the tangential-subloading surface model, in which tangential-inelastic strain rate term makes the inception of bifurcation modes easier in not only normal-yield, but also subyield states. Furthermore, their formation is severely affected by the normal-yield ratio describing the approach of magnitude of stress to that of the normal-yield state.

Keywords: *bifurcation, elastoplasticity, subloading surface mode, tangential plasticity*

1. Introduction

Instability phenomena in elastoplastic solids involve a more or less abrupt change from one deformation pattern to another in the form of localized bifurcation (shear bands) or diffuse bifurcation modes (necking, bulging or buckling). Considerable effort has been devoted over the last decades to gain a comprehensive understanding of the bifurcation phenomena[1)-11)]. Results of these studies suggest the deficiency of traditional elastoplastic constitutive equations in which the interior of yield surface is a purely elastic domain and the plastic strain rate is independent of the stress rate component tangential to the yield/loading surface. Among the existing models describing the tangential stress rate effect[12), 18)], the model proposed by Hashiguchi and Tsutsumi[12)] would be applicable to the arbitrary loading behavior of elastoplastic materials with an arbitrary yield surface. It is formulated by introducing the tangential-inelastic strain rate induced by the deviatoric tangential stress rate tangential to the subloading surface model[13)].

This article explains how the existing bifurcation analyses of deformation in a cylindrical specimen[6)-11)] can be extended to include tangential-subloading surface model. The tangential-subloading surface model is reviewed briefly for incompressible solids, and then based on the constitutive equations; the localized and diffuse bifurcation modes of cylindrical specimen subjected to an axisymmetric load are analyzed. The conditions for the shear band formation, formation of diffuse bifurcations, and long and short wavelength limits of diffuse bifurcation modes are discussed in relation to the material properties and stress.

2. Tangential-Subloading Surface Model

In this section the tangential-subloading surface model, previously proposed by Hashiguchi and Tsutsumi[12)], is reviewed briefly.

Assume the following yield condition with the isotropic hardening

$$f(\boldsymbol{\sigma}) = F(H). \tag{1}$$

The second-order tensor $\boldsymbol{\sigma}$ is the Cauchy stress and H is the isotropic hardening variable.

The elastoplastic constitutive equation will be formulated in the framework of unconventional elastoplasticity in which the interior of the yield surface is not a purely elastic domain but a plastic deformation is induced by the rate of stress inside the yield surface. The subloading surface (see Fig. 1) is described as

$$f(\boldsymbol{\sigma}) = RF(H). \tag{2}$$

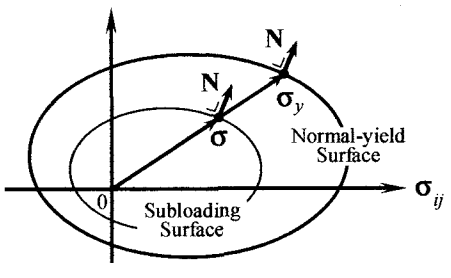

Fig. 1. Normal-yield and subloading surface

The degree of approach to the normal-yield state can be described by the *normal-yield ratio* $R(0 \le R \le 1)$ which is the size of the subloading surface to that of the normal-yield surface.

Let it be assumed that the strain rate $\mathbf{D}$ (the symmetric part of the velocity gradient) is additively decomposed into the elastic strain rate $\mathbf{D}^e$ and the inelastic strain rate $\mathbf{D}^i$ which is further decomposed into the plastic strain rate $\mathbf{D}^p$ and the tangential-inelastic strain rate $\mathbf{D}^t$, i.e.

$$\mathbf{D} = \mathbf{D}^e + \mathbf{D}^i, \tag{3}$$

$$\mathbf{D}^i = \mathbf{D}^p + \mathbf{D}^t, \tag{4}$$

where the elastic strain rate $\mathbf{D}^e$ is given by

$$\mathbf{D}^e = \mathbf{E}^{-1}\overset{\circ}{\boldsymbol{\sigma}}, \tag{5}$$

and the plastic strain rate $\mathbf{D}^p$ due to the associated flow rule is given as

$$\mathbf{D}^p = \lambda \mathbf{N}, \tag{6}$$

$$\lambda = \frac{\mathrm{tr}(\mathbf{N}\overset{\circ}{\boldsymbol{\sigma}})}{M_p}, \tag{7}$$

$$\mathbf{N} = \frac{\partial f}{\partial \boldsymbol{\sigma}} \Big/ \left\| \frac{\partial f}{\partial \boldsymbol{\sigma}} \right\|, \quad (\|\mathbf{N}\| = 1). \tag{8}$$

$\| \ \|$ indicates the magnitude and $(\circ)$ is a proper corotational rate with objectivity. The fourth-order tensor $\mathbf{E}$, the second order tensor $\mathbf{N}$ and M_p are the elastic modulus (Hooke's type), the normalized outward-normal of the subloading surface and the plastic modulus, respectively. $\mathbf{D}^t$ in Eq. (4) is called the tangential-inelastic strain rate and induced by the stress rate component tangential to the subloading surface as illustrated in Fig. 2 for the case of von Mises yield surface, namely the *tangential-stress rate* $\overset{\circ}{\boldsymbol{\sigma}}{}^*_t$. $\mathbf{D}^t$ and $\overset{\circ}{\boldsymbol{\sigma}}{}^*_t$ are formulated as

$$\mathbf{D}^t = \frac{1}{M_t}\overset{\circ}{\boldsymbol{\sigma}}{}^*_t, \tag{9}$$

where

$$M_t = TR^{-b}, \tag{10}$$

$$\overset{\circ}{\boldsymbol{\sigma}}{}^*_t = \overset{\circ}{\boldsymbol{\sigma}}{}^* - \overset{\circ}{\boldsymbol{\sigma}}{}^*_n, \quad \overset{\circ}{\boldsymbol{\sigma}}{}^*_n = \mathrm{tr}(\mathbf{N}\overset{\circ}{\boldsymbol{\sigma}}{}^*\mathbf{N}). \tag{11}$$

$(\ )^*$ stands for the deviatoric part, M_t is a monotonically decreasing function of R, called the tangential-inelastic modulus. $T(>0)$ and $b(\ge 1)$ being material constants.

The stress rate-strain rate relation in the present model for plastically incompressible materials is given as

$$\overset{\circ}{\boldsymbol{\sigma}} = \frac{M_t}{M_t + 2G}\left\{\mathbf{ED} - \frac{\mathrm{tr}(\mathbf{NED})}{M_p + \mathrm{tr}(\mathbf{NEN})}\left(\mathbf{EN} - 2G\frac{M_p}{M_t}\mathbf{N}\right) + \frac{2G}{3M_t}\mathrm{tr}(\mathbf{ED})\mathbf{I}\right\}. \tag{12}$$

where $\mathrm{tr}(\ )$, $\mathbf{I}$ and G are the trace, the identity tensor and the shear modulus, respectively. Hereinafter, let the Zaremba-Jaumann rate be used for the corotational rate of the stress $\boldsymbol{\sigma}$, i.e.

$$\overset{\circ}{\boldsymbol{\sigma}} = \dot{\boldsymbol{\sigma}} + \boldsymbol{\sigma}\mathbf{W} - \mathbf{W}\boldsymbol{\sigma}. \tag{13}$$

$\mathbf{W}$ is the spin tensor (the skew-symmetric part of the velocity gradient) and $(\bullet)$ stands for the material-time derivative.

The positive proportionality factor in the associated flow rule (6) is expressed in terms of the strain rate $\mathbf{D}$, rewriting λ by Λ, as follows:

$$\Lambda = \frac{\mathrm{tr}(\mathbf{NED})}{M_p + \mathrm{tr}(\mathbf{NEN})}, \tag{14}$$

Then, the loading criterion can be given by the positiveness of the proportionality factor as follows[13]:

$$\left.\begin{aligned} &\mathbf{D}^p \ne \mathbf{0}: \ \Lambda > 0, \\ &\mathbf{D}^p = \mathbf{0}: \ \Lambda \le 0. \end{aligned}\right\} \tag{15}$$

The plastic strain rate (6) with Eq. (7) are obtained by substituting the associated flow rule (6) into the consistency condition which is obtained by incorporating the evolution rule of the normal-yield ratio R into the time-differentiation of Eq. (2) for the subloading surface. The plastic loading process develops gradually as the stress approaches the yield surface, exhibiting a smooth elastic-plastic transition.

Adopt the simple elastoplastic material possessing the following von Mises yield condition with linear isotropic hardening[16].

$$f(\boldsymbol{\sigma}) = \sqrt{3/2}\,\|\boldsymbol{\sigma}^*\| = RF, \quad \mathbf{N} = \frac{\boldsymbol{\sigma}^*}{\|\boldsymbol{\sigma}^*\|}, \tag{16}$$

$$F = F_0 + c_i H, \quad \dot{H} = \sqrt{2/3}\,\|\mathbf{D}^p\|, \tag{17}$$

$$M_p = (2/3)c_i R + \sqrt{2/3}UF, \quad U = -u_R \ln R. \tag{18}$$

where c_i and u_R are the material constants and F_0 is the initial value of function F.

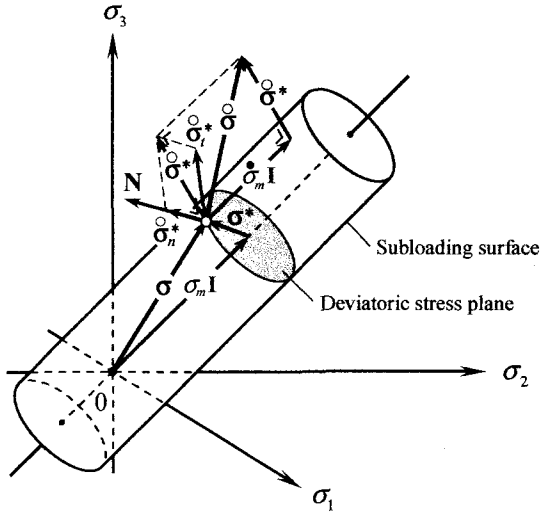

Fig. 2. Tangential stress rate for von Mises yield surface in the principle stress space

3. Bifurcation Analysis

The localized and diffuse necking or bulging modes of the cylindrical specimen subjected to tensile or compressive loading are analyzed by adopting the tangential-subloading surface model in this section.

3.1 Constitutive relations

Consider a circular cylindrical specimen subjected to axial stress σ_{zz} at the frictionless ends, which yields the axisymmetric deformations (see Fig. 3). Deformation is postulated to be homogeneous up to the onset of bifurcation. Let the radius and the height be denoted by $\mathcal{R}$ and $\mathcal{H}$, respectively. The constitutive relationship, Eq. (12), can be expressed in the cylindrical coordinate system as follows:

$$\left.\begin{aligned} &\overset{\circ}{\sigma}_{zz} - \frac{1}{2}(\overset{\circ}{\sigma}_{rr} + \overset{\circ}{\sigma}_{\theta\theta}) = 2\mu^*(D_{zz} - \frac{1}{2}(D_{rr} + D_{\theta\theta})), \\ &\overset{\circ}{\sigma}_{rr} - \overset{\circ}{\sigma}_{\theta\theta} = 2\mu(D_{rr} - D_{\theta\theta}), \\ &\overset{\circ}{\sigma}_{rz} = 2\mu D_{rz}, \end{aligned}\right\} \quad (19)$$

where

$$D_{rr} + D_{\theta\theta} + D_{zz} = 0, \quad D_{r\theta} = D_{\theta z} = 0. \quad (20)$$

The instantaneous shear moduli μ^* and μ are given as follows:

$$\mu^* = G\frac{M_p}{M_p + 2G} (\leq G), \quad (21)$$

$$\mu = G\frac{M_t}{M_t + 2G} (\leq G). \quad (22)$$

The instantaneous shear modulus μ^* in Eq. (21) is independent of the tangential-inelastic strain rate and gradually decreases from the elastic shear modulus G as the normal-yield ratio R increases, as shown in Fig. 4. The instantaneous shear modulus μ, in Eq. (22) is independent of the plastic strain rate and decreases monotonically with the increase of R, as shown in Fig. 4.

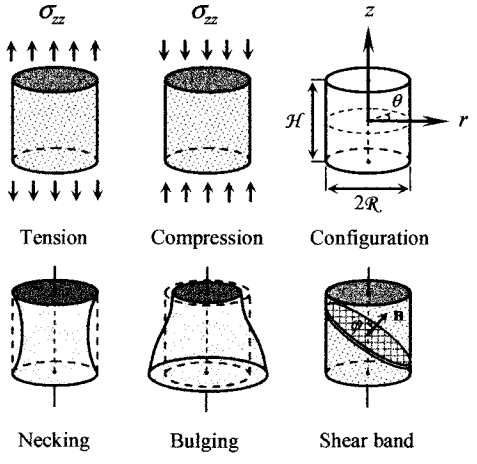

Fig. 3. The cylindrical specimen before and after deformation

A salient feature of the present formulation is that both plastic and tangential-inelastic strain rate are induced gradually as the stress approaches the normal-yield surface, i.e. as $R \to 1$, fulfilling both the continuity and smoothness conditions (Fig. 4). On the other hand, in conventional plasticity models with $u_R \to \infty$ and $T \to \infty$, μ^* and μ suddenly jump from the purely elastic response to the normal-yield response at the moment when the stress reaches the normal-yield surface.

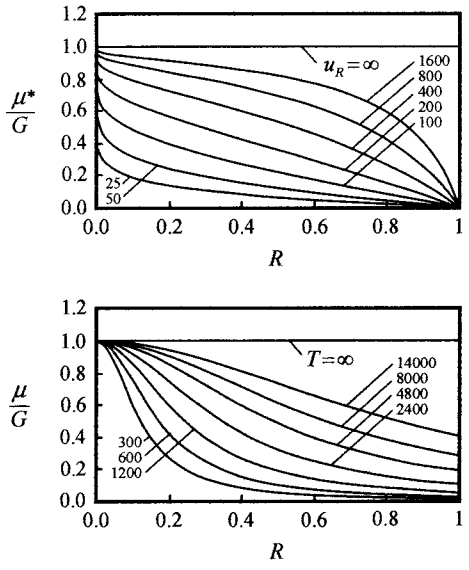

Fig. 4. Instantaneous shear moduli μ^* and μ vs. the normal-yield ratio R, ($c_i = 150$)

3.2 Governing equations

The equilibrium equation can be written as

$$\mathrm{div}\,\dot{\mathbf{\Pi}} = 0, \quad (23)$$

$\dot{\mathbf{\Pi}}$ is called the nominal (*first Piola-Kirchhoff*) stress rate that is related to the *Cauchy stress rate* as

$$\dot{\mathbf{\Pi}} = \dot{\boldsymbol{\sigma}} + (\mathrm{tr}\mathbf{D})\boldsymbol{\sigma} - \boldsymbol{\sigma}\mathbf{L}^{\mathrm{T}}. \quad (24)$$

$\mathbf{L}^{\mathrm{T}}$ is the transpose of velocity gradient. By substituting Eq. (13) into Eq. (24), the nominal stress rate $\dot{\mathbf{\Pi}}$ can be rewritten as[19]:

$$\dot{\mathbf{\Pi}} = \overset{\circ}{\boldsymbol{\sigma}} + (\mathrm{tr}\mathbf{D})\boldsymbol{\sigma} - \boldsymbol{\sigma}\mathbf{D} + \mathbf{W}\boldsymbol{\sigma}. \quad (25)$$

For axisymmetric deformations, the strain rate tensor $\mathbf{D}$ and the spin tensor $\mathbf{W}$ are described as

$$\mathbf{D} = \begin{bmatrix} v_{r,r} & 0 & (v_{r,z} + v_{z,r})/2 \\ 0 & r^{-1}v_r & 0 \\ (v_{r,z} + v_{z,r})/2 & 0 & v_{z,z} \end{bmatrix}, \quad (26)$$

$$\mathbf{W} = \begin{bmatrix} 0 & 0 & (v_{r,z} - v_{z,r})/2 \\ 0 & 0 & 0 \\ -(v_{r,z} - v_{z,r})/2 & 0 & 0 \end{bmatrix}. \quad (27)$$

In addition, using Eq. (13) and Eq. (25), we obtain the following equations:

$$\overset{\circ}{\boldsymbol{\sigma}} = \begin{bmatrix} \overset{\bullet}{\sigma}_{rr} & 0 & \overset{\bullet}{\sigma}_{rz} - \sigma(v_{r,z} - v_{z,r}) \\ 0 & \overset{\bullet}{\sigma}_{\theta\theta} & 0 \\ \overset{\bullet}{\sigma}_{zr} - \sigma(v_{r,z} - v_{z,r}) & 0 & \overset{\bullet}{\sigma}_{zz} \end{bmatrix}, \quad (28)$$

$$\overset{\bullet}{\boldsymbol{\Pi}} = \begin{bmatrix} \overset{\circ}{\sigma}_{rr} & 0 & \overset{\circ}{\sigma}_{rz} + \sigma(v_{r,z} - v_{z,r}) \\ 0 & \overset{\circ}{\sigma}_{\theta\theta} & 0 \\ \overset{\circ}{\sigma}_{zr} - \sigma(v_{r,z} + v_{z,r}) & 0 & \overset{\circ}{\sigma}_{zz} - \sigma_{zz} v_{z,z} \end{bmatrix}, \quad (29)$$

where

$$\sigma = \frac{1}{2}\sigma_{zz}. \quad (30)$$

Bifurcation conditions for axisymmetric loading have been analyzed by Vardoulakis[9] for dry sands; Miles and Nuwayhid[10] for metals, and Chau[11] for rocks. They followed the approach of Cheng et al.[6] for axisymmetric conditions and Hill and Hutchinson[1] for plane strain conditions. In our research, we consider a purely homogeneous deformation process and proceeds up to the inception of bifurcation. We choose the cylindrical polar coordinate system (r, θ, z) such that the origin is located in the center of the cylinder and the z-axis coincides with the axis of symmetry (Fig. 3). At the ends $(z = \pm H/2)$, the specimen are subjected to tensile or compressive loading without shear traction. For the axisymmetric conditions, Eq. (23) reduces to

$$\left.\begin{aligned} &\overset{\bullet}{\Pi}_{rr,r} + \overset{\bullet}{\Pi}_{rz,z} + \frac{1}{r}(\overset{\bullet}{\Pi}_{rr} + \overset{\bullet}{\Pi}_{\theta\theta}) = 0, \\ &\overset{\bullet}{\Pi}_{zz,z} + \overset{\bullet}{\Pi}_{zr,r} + \frac{1}{r}\overset{\bullet}{\Pi}_{zr} = 0. \end{aligned}\right\} \quad (31)$$

Differentiating and combining the two relationships in Eq. (31) to eliminate $\overset{\bullet}{\Pi}_{zz} + \overset{\bullet}{\Pi}_{rr}$, we obtain an expression in terms of the gradient of velocities using Eq. (29). Introducing the stream function $\Psi(r, z)$, it results in

$$v_r = \Psi_{,z}, \qquad v_z = -\frac{1}{r}(r\Psi)_{,r}. \quad (32)$$

By substituting Eqs. (29) and (32) into Eq. (31), along with constitutive relations in Eq. (19), we obtain

$$(\mu - \sigma)O_r^2(\Psi) + (3\mu^* - \mu)(O_r(\Psi))_{,zz} + (\mu + \sigma)\Psi_{,zzzz} = 0, \quad (33)$$

where the operator O_r is defined as follows:

$$O_r(\ ) = (\frac{1}{r}(r\ )_{,r})_{,r}. \quad (34)$$

Eq. (33) is a fourth-order partial differential equation of the mixed type that can be the elliptic, hyperbolic or parabolic depending on the state of stress and values of internal variables. The particular linearization described here yields a governing equation applicable to the subloading surface model with tangential stress rate effect. Our analyses of axisymmetric bifurcation modes in elastic-plastic incompressible cylinders have the similar form as that obtained by Cheng et al.[6], Hutchinson and Miles[8], Vardoulakis[9], Miles and Nuwayhid[10] and Chau[11]. The similar conclusion was reached from the corresponding bifurcation analyses under the plane strain conditions done by Hill and Hutchinson[1], Young[2], Needleman[3], Vardoulakis[4], Chau and Rudnicki[5], and Hashiguchi and Khojastehpour[15].

3.3 Localized bifurcation

The shear band formation conditions at the onset of strain localization are analyzed in this section.

Consider a purely homogeneous deformation process, progressing to the onset of shear band formation, at which the principal stress axes coincide with the coordinate axes r and z. The unit vector normal to a shear band is denoted by $\mathbf{n}(r, z)$ with $n_\theta = 0$ such that the shear band inclines against the z-axis (Fig. 3). Two conditions must be satisfied for the shear band formation: 1) geometrical compatibility which requires the velocity increment to be continuous but permits a jump in the velocity gradient across the shear band, and 2) the incremental equilibrium across the shear band[17]. These conditions can be expressed as follows:

$$v_{i,j} = g_i n_j, \qquad \overset{\bullet}{\Pi}_{ij} n_j = 0, \qquad (i, j = r, z). \quad (35)$$

$\mathbf{g}$ is the jump vector of the velocity gradient and $\mathbf{n}$ is the unit vector normal to the shear band. Substituting Eq. (29) into (35) with constitutive relations (19) yields the following fourth-order algebraic equation:

$$(\mu - \sigma)n_r^4 + (3\mu^* - \mu)n_r^2 n_z^2 + (\mu + \sigma)n_z^4 = 0. \quad (36)$$

The condition for the formation of shear band is given as a loss of ellipticity of Eq. (36). The solutions of n_r/n_z in Eq. (36) are classified as the elliptic complex (EC), elliptic imaginary (EI), parabolic (P) and hyperbolic (H) regimes, according to the existence of zero, two, and four real roots, respectively for Eq. (36). Regimes with restrictions $\mu^* > 0$, $\mu > 0$ and $\sigma > 0$ may be classified as

Elliptic complex regime:

$$\left(\frac{\mu}{3\mu^*} + \frac{1}{3}\right)^2 > \frac{4}{3}\left(\left(\frac{\sigma}{3\mu^*}\right)^2 + \frac{1}{3}\right). \quad (37)$$

Elliptic imaginary regime:

$$\left(\frac{\mu}{3\mu^*} + \frac{1}{3}\right)^2 < \frac{4}{3}\left(\left(\frac{\sigma}{3\mu^*}\right)^2 + \frac{1}{3}\right), \quad \mu > \sigma, \ 3\mu^* > \mu. \quad (38)$$

Parabolic regime:

$$\mu < \sigma. \quad (39)$$

Hyperbolic regime:

$$\left(\frac{\mu}{3\mu^*}+\frac{1}{3}\right)^2 < \frac{4}{3}\left(\left(\frac{\sigma}{3\mu^*}\right)^2+\frac{1}{3}\right),\ \mu>\sigma,\ 3\mu^*<\mu. \quad (40)$$

Let it be assumed that the shear band will be formed at the instant that the $(\sigma/3\mu^*, \mu/3\mu^*)$ trajectory passes through the EC-H boundary. The inclination angle φ of the shear band, i.e. the angle measured in anti-clockwise direction from the maximum principal stress (σ_{zz}) direction to the direction normal to the shear band can be written from Eq. (36) as

$$\varphi \equiv \tan^{-1}\left(\frac{n_r}{n_z}\right) = \tan^{-1}\sqrt{-\frac{3\mu^*-\mu}{2(\mu-\sigma)}}. \quad (41)$$

Here, when the trajectory directly passes though the E-P boundary $(\mu=\sigma, 3\mu^*>\mu)$ with $n_z=0$ produced by Eq. (36), and the direction of the shear band is unrealistically predicted to be perpendicular to the maximum principal stress direction, i.e. $\varphi=\pi/2$. Therefore, one is limited to the EC-H boundary when calculating shear band formation.

3.4 Diffuse bifurcation modes

Diffuse necking or bulging modes as the axisymmetric bifurcation appearing in the elliptic, hyperbolic and parabolic regimes are considered in this section. Special limits of diffuse modes such as the long wavelength and the short wavelength limit are emphasized.

We investigate the possibility of diffuse bifurcations that precede localization for a cylindrical incompressible specimen with radius $\mathcal{R}$ and height $\mathcal{H}$ at the onset of bifurcation (Fig. 3). The specimen is subjected to current axial compressive or tensile stress σ_{zz} at the ends without friction. The stream function $\Psi(r,z)$, which gives rise to the diffuse bifurcation modes is given by

$$\Psi(r,z)=\psi(r)\cos(\zeta z), \quad (42)$$

where $\zeta = m\pi/\mathcal{H}$ and $m=1,2,3,\ldots$. The substitution of Eq. (42) into Eq. (32) results in

$$\left.\begin{aligned} v_r &= -\psi(r)\zeta\sin(\zeta z),\\ v_z &= -(d\psi(r)/dr+\psi(r)/r)\cos(\zeta z). \end{aligned}\right\} \quad (43)$$

The boundary conditions for axisymmetric deformations can be written as

$$\left.\begin{aligned} &v_z=0, \quad \overset{\bullet}{\Pi}_{rz}=0, \quad \text{on the ends } (z=\pm\mathcal{H}/2),\\ &\overset{\bullet}{\Pi}_{rr}=0, \quad \overset{\bullet}{\Pi}_{zr}=0, \quad \text{on the sides } (r=\mathcal{R}). \end{aligned}\right\} \quad (44)$$

The substitution of Eqs. (19), (20), (42) and (44) into Eq. (31) leads to the boundary conditions on the sides to be expressed as

$$\left.\begin{aligned} &O_r(\psi)+\zeta^2\psi=0,\\ &(\mu-\sigma)d(rO_r(\psi))/rdr-\zeta^2((3\mu^*-\sigma)d\psi/dr\\ &\qquad +(3\mu^*-2\mu-\sigma)\psi/r)=0. \end{aligned}\right\} \quad (45)$$

If one substitutes the eigenmode of Eq. (42) into Eq. (33), the following governing differential equation can be obtained:

$$(\mu-\sigma)O_r^2(\psi)-\zeta^2(3\mu^*-\mu)O_r(\psi) +\zeta^4(\mu+\sigma)\psi=0, \quad (46)$$

Alternatively, Eq. (46) can be written as:

$$(O_r+\zeta^2\Upsilon_1^2)(O_r+\zeta^2\Upsilon_2^2)\psi(r)=0. \quad (47)$$

Further, it can be written as two Bessel's differential equations with respect to Υ_1 and Υ_2. Since $\psi(r)$ should be finite at $r=0$, the general solutions of Eq. (46) or Eq. (47) have the form

$$\psi(r)=MJ_1(\zeta\Upsilon_1 r)+NJ_1(\zeta\Upsilon_2 r), \quad (48)$$

where M and N are constants. $J_1(\ )$ is the Bessel function of the first kind and the first order, and Υ_1 and Υ_2 are the roots of the following characteristic equation.

$$(\mu-\sigma)\Upsilon^4+(3\mu^*-\mu)\Upsilon^2+(\mu+\sigma)=0. \quad (49)$$

The roots of Eq. (49) are classified into the elliptic complex (EC), the elliptic imaginary (EI), the hyperbolic (H) and the parabolic (P) regimes, dependenting on the state of stress and values of internal variables. In each of these regimes, diffuse bifurcations are possible, and in each regime the analysis leads to the appropriate eigenvalue equation. The solutions of the eigenvalue equations are similar to that of equations for plane strain conditions by Hill and Hutchinson[1] and for axisymmetric deformations by Vardoulakis[9] and Chau[11]. The results by the subloading surface model with tangential stress rate, which we incorporate in the present study, are summarized below.

Elliptic complex regime:

The solution (48) in the elliptic complex regime has the form

$$\psi(r)=\mathrm{Re}\left[MJ_1(\zeta\Upsilon r)\right], \quad (50)$$

Re[ ] denotes the real part of [ ]. $\Upsilon=p+iq$, $(i=\sqrt{-1})$, and its conjugate $\bar{\Upsilon}=p-iq$ are the roots of Eq. (49). Substituting Eq. (50) into boundary conditions of Eq. (45) leads to the following eigenvalue equation:

$$\frac{(\Upsilon^2-1)J_1(\omega\Upsilon)}{(\bar{\Upsilon}^2-1)J_1(\omega\bar{\Upsilon})} = \frac{\omega\Upsilon((\mu-\sigma)\Upsilon^2+(3\mu^*-\sigma))J_0(\omega\Upsilon)-2\mu J_1(\omega\Upsilon)}{\omega\bar{\Upsilon}((\mu-\sigma)\bar{\Upsilon}^2+(3\mu^*-\sigma))J_0(\omega\bar{\Upsilon})-2\mu J_1(\omega\bar{\Upsilon})}, \quad (51)$$

Alternatively, Eq. (51) can be written as

$$\mathrm{Im}\left[(\bar{\Upsilon}^2-1)J_1(\omega\bar{\Upsilon})\{\omega\Upsilon((\mu-\sigma)\Upsilon^2 +(3\mu^*-\sigma))J_0(\omega\Upsilon)-2\mu J_1(\omega\Upsilon)\}\right]=0, \quad (52)$$

where Im[ ] denotes the imaginary part of [ ] and $\omega=\zeta\mathcal{R}=m\pi\mathcal{R}/\mathcal{H}$ is the wavelength. The quantities p and q satisfy the following equations:

$$\left.\begin{aligned} p^2+q^2 &= ((\mu+\sigma)/(\mu-\sigma))^{1/2}, \\ p^2-q^2 &= -(3\mu^*-\mu)/(2(\mu-\sigma)). \end{aligned}\right\} \quad (53)$$

Elliptic imaginary regime:

The general solutions, Eq. (48), in the elliptic imaginary regime have the form

$$\psi(r) = MI_1(\zeta pr) + NI_1(\zeta qr), \quad (54)$$

where $I_1(\ )$ is the modified Bessel function of the first kind and the first order. In the elliptic imaginary regime, the roots of Eq. (49) are $\Upsilon_1 = ip$ and $\Upsilon_2 = iq$. The substitution of Eq. (54) into the boundary conditions (45) yields the eigenvalue equation:

$$\frac{(p^2+1)I_1(\omega p)}{(q^2+1)I_1(\omega q)} = \frac{\omega p((\mu-\sigma)p^2-(3\mu^*-\sigma))I_0(\omega p)+2\mu I_1(\omega p)}{\omega q((\mu-\sigma)q^2-(3\mu^*-\sigma))I_0(\omega q)+2\mu I_1(\omega q)}, \quad (55)$$

where p and q satisfy the following equations:

$$\left.\begin{aligned} p^2+q^2 &= (3\mu^*-\mu)/(\mu-\sigma), \\ p^2-q^2 &= ((3\mu^*-\mu)^2-4(\mu^2-\sigma^2))^{1/2}/(\mu-\sigma). \end{aligned}\right\} \quad (56)$$

Parabolic regime:

The general solutions, Eq. (48), in the parabolic regime have the form

$$\psi(r) = MJ_1(\zeta pr) + NI_1(\zeta qr), \quad (57)$$

where $\Upsilon_1 = p$ and $\Upsilon_2 = iq$ are the roots of Eq. (49) for the parabolic regime. Substitution of Eq. (57) into the boundary conditions (45) yields the eigenvalue equation:

$$\frac{(p^2-1)J_1(\omega p)}{(q^2+1)I_1(\omega q)} = \frac{\omega p((\mu-\sigma)p^2+(3\mu^*-\sigma))J_0(\omega p)-2\mu J_1(\omega p)}{\omega q((\mu-\sigma)q^2-(3\mu^*-\sigma))I_0(\omega q)+2\mu I_1(\omega q)}, \quad (58)$$

where p and q satisfy

$$\left.\begin{aligned} p^2+q^2 &= ((3\mu^*-\mu)^2-4(\mu^2-\sigma^2))^{1/2}/|\mu-\sigma|, \\ p^2-q^2 &= -(3\mu^*-\mu)/(\mu-\sigma). \end{aligned}\right\} \quad (59)$$

Hyperbolic regime:

Solution (48) in the hyperbolic regime has the form

$$\psi(r) = MJ_1(\zeta pr) + NJ_1(\zeta qr), \quad (60)$$

In the hyperbolic regime, the roots of Eq. (49) are $\Upsilon_1 = p$ and $\Upsilon_2 = q$. The substitution of Eq. (60) into the boundary conditions of Eq. (45) yields the eigenvalue equation:

$$\frac{(p^2-1)J_1(\omega p)}{(q^2-1)J_1(\omega q)} = \frac{\omega p((\mu-\sigma)p^2+(3\mu^*-\sigma))J_0(\omega p)-2\mu J_1(\omega p)}{\omega q((\mu-\sigma)q^2+(3\mu^*-\sigma))J_0(\omega q)-2\mu J_1(\omega q)}, \quad (61)$$

where p and q are defined as

$$\left.\begin{aligned} p^2+q^2 &= -(3\mu^*-\mu)/(\mu-\sigma), \\ p^2-q^2 &= ((3\mu^*-\mu)^2-4(\mu^2-\sigma^2))^{1/2}/(\mu-\sigma). \end{aligned}\right\} \quad (62)$$

Since localized bifurcation can be seen in the materials and diffuse bifurcation modes occur before localization, the discussion about geometrical diffuse modes is important. Fig. 5 represents the bifurcation regimes as a function of the dimensionless variables $\sigma/3\mu^*$ and $\mu/3\mu^*$ by the specified regions. Fig. 5 shows that the bifurcation domains coincide for compressive and tensile stress. The geometric diffuse bifurcation modes appear in the elliptic, hyperbolic and parabolic regimes.

Fig. 6 represents the lowest bifurcation stress as a function of the wavelength of diffuse modes $\omega = m\pi\mathcal{R}/\mathcal{H}$ obtained for axisymmetric elliptic modes of bifurcation in several values of $3\mu^*/\mu$, in which the long wavelength limit $\omega \to 0$ coincides with the $\sigma/3\mu^*$-axis. The lowest possible bifurcation stress is induced at $\omega = 0$, rising more rapidly when ω is in-between one and three for tensile loading and two and four for compressive loading, then slowly turns down as a value of ω increases. Here, it should be noted that the eigenvalue surface has a maximum point that occurs at ω in-between one and four.

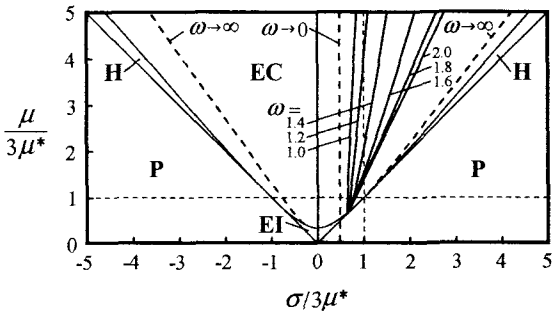

Fig. 5. Characteristic regimes and $(\sigma/3\mu^*, \mu/3\mu^*)$ trajectories

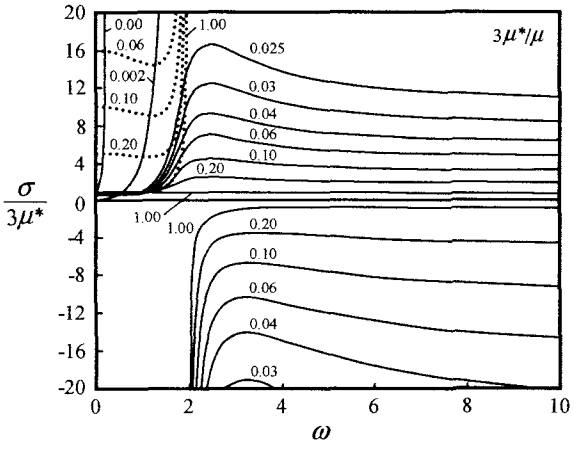

Fig. 6. Lowest bifurcation stresses with the variation of $3\mu^*/\mu$

3.5 Long and short wavelength diffuse modes

We consider here the long wavelength limit ($\omega \to 0$) and the short wavelength limit ($\omega \to \infty$) of the eigenvalue equation in EC, EI, P and H regimes.

In the elliptic complex regime, dividing the numerator and the denominator for both sides of Eq. (51) to $J_1(\omega\Upsilon)$ and $J_1(\omega\bar{\Upsilon})$, respectively, and with $\lim_{\omega\to 0}\omega\Upsilon J_0(\omega\Upsilon)/J_1(\omega\Upsilon)=2$ and $\lim_{\omega\to 0}\omega\bar{\Upsilon}J_0(\omega\bar{\Upsilon})/J_1(\omega\bar{\Upsilon})=2$, yields the following simplified equation:

$$\frac{\sigma}{3\mu^*}=\frac{1}{2}. \tag{63}$$

Alternatively, when $J_0(\ )$ and $J_1(\ )$ are written as the series representation[20], then for small values of ω and the first two terms, Eq. (51) can be factored as follows:

$$\frac{\sigma}{3\mu^*}=\frac{1}{2}+\frac{1}{2^4}\omega^2\Big[\Big(1+\frac{\mu}{3\mu^*}-3\frac{\sigma}{3\mu^*}\Big)\Big(\frac{3\mu^*-\sigma}{\mu-\sigma}\Big) -\Big(1-\frac{\mu}{3\mu^*}-2\frac{\sigma}{3\mu^*}\Big)\Big] +\frac{1}{2^6}\omega^4\Big(1+\frac{1}{2}\frac{\mu}{3\mu^*}-2\frac{\sigma}{3\mu^*}\Big)\Big(\frac{\mu+\sigma}{\mu-\sigma}\Big). \tag{64}$$

The substitution of the asymptotic expansions of $J_0(\ )$ and $J_1(\ )$ with large arguments[20] into Eq. (51), for the short wavelength limit ($\omega \to \infty$) in the elliptic complex regime, yields

$$\frac{\sigma}{3\mu^*}=\frac{1}{2}+\frac{1}{2}\frac{\mu}{3\mu^*}+\frac{\sigma}{3\mu^*}\Big(\frac{\mu-\sigma}{\mu+\sigma}\Big)^{1/2}. \tag{65}$$

The ($\sigma/3\mu^*$, $\mu/3\mu^*$) trajectories of the EC regime for the typical wavelength ω ranging from 1.0 to 2.0 are depicted in Fig. 5. Taking into account that diffuse bifurcation modes are observed for ω in-between 1.0 and 2.0, it can be shown that the wavelength ω is near the peak of the eigenstress by the numerical results (see Fig. 6). The ($\sigma/3\mu^*$, $\mu/3\mu^*$) trajectories for the long wavelength limit ($\omega \to 0$) (Eq. (63)) and the short wavelength limit ($\omega \to \infty$) (Eq. (65)) are shown in Fig. 5 by the dashed line and curves, respectively.

Considering the elliptic imaginary regime in the long wavelength limit ($\omega \to 0$), dividing the numerator and the denominator in both sides of Eq. (55) to $I_1(\omega p)$ and $I_1(\omega q)$, respectively, and noting that $\lim_{\omega\to 0}\omega p I_0(\omega p)/I_1(\omega p)=2$ and $\lim_{\omega\to 0}\omega q I_0(\omega q)/I_1(\omega q)=2$, again leads to Eq. (63). The substitution of the first two terms in the series representation of the modified Bessel functions $I_0(\ )$ and $I_1(\ )$[20] into Eq. (55) for small values of ω, again yields Eq. (64). In the short wavelength limit ($\omega \to \infty$), the substitution of the asymptotic expansions of $I_0(\ )$ and $I_1(\ )$ for large arguments[20] into Eq. (55), again produces Eq. (65). Therefore, the long wavelength and the short wavelength bifurcation modes continue to appear across the EC-EI boundary.

In the parabolic regime, using the same argument used by Chau[11], bifurcation of diffuse modes becomes possible as soon as the parabolic regime is entered considering Eq. (58). This relation is found to be similar to that for the parabolic eigenvalue equation for a rectangular specimen under plane strain deformations. Consequently, the arguments employed by Hill and Hutchison[1] and Needleman[3] for the eigenvalue equation on the tensile elliptic-parabolic boundary in the plane strain condition can be also applied here. Therefore, the same argument applies identically for the compressive elliptic-parabolic boundary. In particular, there is an infinite sequence of eigenvalues available in the vicinities of both the tensile and compressive E-P boundaries for some sufficiently large ω. Therefore, short wavelength diffuse modes and shear band modes are always available simultaneously once the parabolic regime is entered.

In the hyperbolic regime, expansion of (61) for small ω leads again to Eq. (63). Hence, the long wavelength necking and bulging modes continue through the elliptic-hyperbolic boundary. In the short wavelength limit ($\omega \to \infty$), the substitution of the asymptotic expansions of $J_0(\ )$ and $J_1(\ )$ for large arguments[20] into Eq. (61), again produces Eq. (65). Consequently, the bifurcation into some sufficiently short wavelength mode is possible as soon as the hyperbolic region is entered.

Although geometric diffuse modes in both hyperbolic and parabolic regimes are found to be mathematically admissible, they are of less interest and elliptic diffuse modes may play a significant role in the development of subsequent localization.

4. Concluding Remarks

Instantaneous shear moduli, shear band formation and diffuse bifurcation modes of a cylindrical incompressible specimen subjected to axisymmetric compression and tension were analyzed incorporating the tangential-subloading surface model. The main results are summarized here.

1) Analytical solutions for the inception of localized bifurcation and diffuse bifurcation modes were derived and classified into the elliptic complex, elliptic imaginary, hyperbolic and the parabolic regimes.
2) The localized and diffuse bifurcation of deformation can simulated well by the tangential-subloading surface mode, and thus is revealed that pre-peak bifurcation of diffuse modes is always possible and can occur preceding the formation of localization mode.
3) Incorporation of the tangential-inelastic strain rate has no influence on the instantaneous shear moduli μ^*, but lowers the instantaneous shear moduli μ.
4) The tangential-inelastic strain rate term satisfies conditions necessary for bifurcations for both normal-yield and subyield states.
5) The formation of shear band and diffuse bulging or necking modes is affected markedly by the normal-yield ratio describing the approach of stress to the normal-yield state.

Acknowledgment

This research has been supported by Postdoctoral Fellowship of the Japan Society for the Promotion of Science (JSPS) for Foreigner Researchers.

References

1) Hill, R. and Hutchinson, J.W., Bifurcation phenomena in the plane tension test, *J. Mech. Phys. Solids*, Vol. 23, pp. 239-264, 1975.
2) Young, N. J. B., Bifurcation phenomena in plane compression test, *J. Mech. Phys. Solids*, Vol. 24, pp. 77-91, 1976.
3) Needleman, A., Non-normality and bifurcation in plane strain tension and compression, *J. Mech. Phys. Solids*, Vol. 27, pp. 231-254, 1979.
4) Vardoulakis, I., Bifurcation analysis of the plane rectilinear deformation on dry sand samples, *Int. J. Solids Struct.*, Vol. 17, pp. 1085-1101, 1981.
5) Chau, K.T, and Rudnicki, J.W., Bifurcation of compressible pressure-sensitive materials in plane strain tension and compression, *J. Mech. Phys. Solids*, Vol. 38, pp. 875-898, 1990.
6) Cheng, S.Y., Ariaratnam, S.T. and Dubey, R.N., Axisymmetric bifurcation in an elastic-plastic cylinder under axial load and lateral hydrostatic pressure, *Quart. Appl. Math.*, Vol. 29, pp. 41-51, 1971.
7) Miles, J.P., Bifurcation in plastic flow under uniaxial tension, *J. Mech. Phys. Solids*, Vol. 19, pp. 89-102. 1971.
8) Hutchinson, J.W. and Miles, J.P., Bifurcation analysis of the onset of necking in an elastic/plastic cylinder under uniaxial tension, *J. Mech. Phys. Solids*, Vol. 22, pp. 61-71, 1974.
9) Vardoulakis, I., Rigid granular plasticity model and bifurcation in triaxial test, *Acta Mechanica*, Vol. 49, pp. 57-79, 1983.
10) Miles, J.P. and Nuwayhid, U.A., Bifurcation in compressible elastic/plastic cylinders under uniaxial tension, *Appl. Sci. Res.*, Vol. 42, pp. 33-54, 1985.
11) Chau, K.T., Non-normality and bifurcation in a compressible pressure-sensitive circular cylinder under axisymmetric tension and compression, *Int. J. of Solids Struct.*, Vol. 29, pp. 801-824, 1992.
12) Hashiguchi, K. and Tsutsumi, S., Elastoplastic constitutive equation with tangential stress rate effect, *Int. J. Plasticity*, Vol. 17, pp. 117-145, 2001.
13) Hashiguchi, K., Saitoh, K., Okayasu, T. and Tsutsumi, S., Evaluation of typical conventional and unconventional plasticity models for prediction of softening behavior of soils, *Geotechnique*, 52, pp. 561-573, 2002.
14) Hashiguchi, K. and Tsutsumi, S., Shear band formation analysis in soils by the subloading surface model with tangential stress rate effect, *Int. J. Plasticity*, Vol. 19, pp. 1651-1677, 2003.
15) Hashiguchi, K. and Khojastehpour, M., Bifurcation analysis of diffuse modes by the subloading surface model with tangential stress rate effect, *J. Appl. Mech., JSCE*, Vol. 6, pp. 513-520, 2003.
16) Hashiguchi, K. and Protasov, A., Localized necking analysis by the subloading surface model with tangential-strain rate and anisotropy, *Int. J. Plasticity*, 2004, in press.
17) Hill, R., Discontinuity relations in mechanics of solids, *Progress in Solid Mechanics,* Vol. 2, pp. 246-276, 1961.
18) Rudnicki, J.W. and Rice, J.R., Conditions for localization of deformation in pressure-sensitive dilatant materials, *J. Mech. Phys. Solids*, Vol. 23, pp. 371-394, 1975.
19) Yatomi, C., Yashima, A., Iizuka, A. and Sano, I., General theory of shear bands formation by a non-coaxial Cam-clay model, *Soils and Found.*, Vol. 29, pp. 41-53, 1989.
20) Spiegel, M.R. and Liu, J., *Mathematical handbook of formulas and tables*, Schaum's outline series, McGraw-Hill, USA, 1999.

(Received: April 16, 2004)